Neighboring Group Participation in the Transition State of Human Purine Nucleoside Phosphorylase†

Andrew S. Murkin, Matthew R. Birck,‡ Agnes Rinaldo-Matthis, Wuxian Shi,§ Erika A. Taylor, Steven C. Almo, and Vern L. Schramm*

Department of Biochemistry, Albert Einstein College of Medicine, 1300 Morris Park Avenue, Bronx, New York 10461

Received January 24, 2007; Revised Manuscript Received February 23, 2007

ABSTRACT: The X-ray crystal structures of human purine nucleoside phosphorylase (PNP) with bound inosine or transition-state analogues show His^{257} within hydrogen bonding distance of the 5′-hydroxyl. The mutants His257Phe, His257Gly, and His257Asp exhibited greatly decreased affinity for Immucillin-H (ImmH), binding this mimic of an early transition state as much as 370-fold (K_m/K_i) less tightly than native PNP. In contrast, these mutants bound DADMe-ImmH, a mimic of a late transition state, nearly as well as the native enzyme. These results indicate that His^{257} serves an important role in the early stages of transition-state formation. Whereas mutation of His^{257} resulted in little variation in the PNP·DADMe-ImmH·SO_4 structures, His257Phe·ImmH·PO_4 showed distortion at the 5′-hydroxyl, indicating the importance of H-bonding in positioning this group during progression to the transition state. Binding isotope effect (BIE) and kinetic isotope effect (KIE) studies of the remote 5′-^{3}H for the arsenolysis of inosine with native PNP revealed a BIE of 1.5% and an unexpectedly large intrinsic KIE of 4.6%. This result is interpreted as a moderate electronic distortion toward the transition state in the Michaelis complex with continued development of a similar distortion at the transition state. The mutants His257Phe, His257Gly, and His257Asp altered the 5′-^{3}H intrinsic KIE to −3, −14, and 7%, respectively, while the BIEs contributed 2, 2, and −2%, respectively. These surprising results establish that forces in the Michaelis complex, reported by the BIEs, can be reversed or enhanced at the transition state.

Determination of the transition-state structure of enzymatic reactions allows for the design of tight binding transition-state analogue inhibitors. These transition-state mimics can subvert the energetics that govern formation of the enzymatic transition state to achieve binding orders of magnitude stronger than that of substrate. The transition-state structures of enzymatic reactions have frequently been established by measuring kinetic isotope effects (KIEs)[1] from the competitive reaction of isotopically labeled substrates. These isotope effects on k_{cat}/K_m, often termed *V*/*K* KIEs (*1*), are a powerful tool in establishing bond vibrational differences between reactants free in solution and at the transition state. Unfortunately, they do not distinguish isotope effects arising from chemistry at the transition state from those generated in the Michaelis complex (Figure 1a). Equilibrium binding isotope effects (BIEs), however, can be measured in separate experiments to determine the extent to which binding contributes to the *V*/*K* KIE (*2*, *3*). Measurement of both BIEs and KIEs permits resolution of binding distortion and bond distortions due to chemistry at the transition state.

The determination of BIEs to help interpret KIE data has recently been applied to thymidine phosphorylase (TP), in which a large secondary ^{3}H KIE of 6.1%, remote from the reaction center, had been found (*4*). The corresponding ^{3}H BIE was subsequently measured to be 6.0%, accounting for the entire *V*/*K* KIE (*2*). Human purine nucleoside phosphorylase (HsPNP) catalyzes the mechanistically similar reversible phosphorolysis of purines (e.g., inosine) to yield ribose 1-phosphate and free nucleobase (e.g., hypoxanthine). By determining the KIEs for the HsPNP-catalyzed arsenolysis reaction (Figure 1b), Lewandowicz and Schramm (*5*) determined the transition-state structure, indicating that the reaction proceeds via an S_N1-like mechanism. As in TP, a large remote secondary 5′-^{3}H KIE of 6.2% was determined for HsPNP. The same question is therefore raised: Is this KIE due primarily to binding interactions or to changes exclusive to the transition state?

Insight into the origin of the remote KIE in the PNP reaction may be obtained by examination of structural features in the proximity of C5′. Human and bovine PNP structures obtained from X-ray crystallography show that the 5′-hydroxyl of the substrate and transition-state analogues is within hydrogen bonding distance of His^{257} (*6*, *7*). It has been hypothesized that this residue is responsible for positioning O5′ in line with O4′ and the nucleophilic oxygen of phosphate (*8*). This "oxygen stack" is proposed to

† Supported by National Institutes of Health Grants GM41916, GM068036 and the Wenner-Gren Foundation.

* To whom correspondence should be addressed. E-mail: vern@aecom.yu.edu. Telephone: (718) 430-2813. Fax: (718) 430-8565.

‡ Current address: Department of Chemistry, Barnard College, 3009 Broadway, New York, NY 10027.

§ Current address: Center for Synchrotron Bioscience, Brookhaven National Laboratory, Upton, NY 11973.

[1] Abbreviations: KIE, kinetic isotope effect; *V*/*K* KIE, kinetic isotope effect on the second-order rate constant, k_{cat}/K_m; BIE, binding isotope effect; HsPNP, human purine nucleoside phosphorylase; PDB, Protein Data Bank; ImmH, Immucillin-H; DADMe-ImmH, 4′-deaza-1′-aza-2′-deoxy-1′-(9-methylene)-Immucillin-H; rms, root-mean-square; TP, thymidine phosphorylase.

10.1021/bi700147b CCC: $37.00
Published on Web 04/04/2007

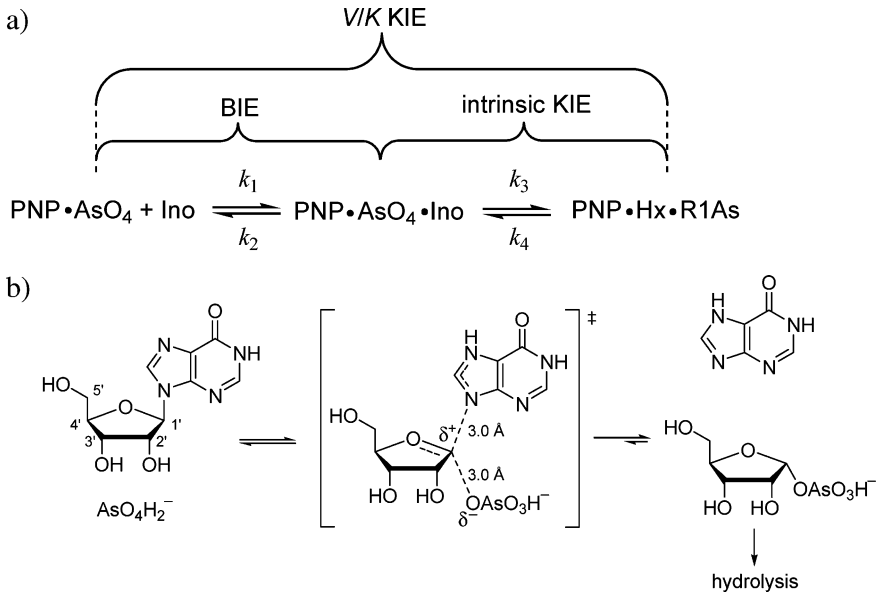

FIGURE 1: (a) Relationship among BIE, *V/K* KIE, and intrinsic KIE using purine nucleoside phosphorylase (PNP) as a model. Ino is inosine, Hx hypoxanthine, and R1As ribose 1-arsenate. (b) Arsenolysis reaction catalyzed by purine nucleoside phosphorylase, including the S_N1-like transition state. Unlike the analogous phosphorolysis reaction, arsenolysis is irreversible due to the instability of the ribose 1-arsenate product, which rapidly hydrolyzes. N7 of the leaving group has been depicted as being protonated at the transition state, as this has been demonstrated to be a common mechanistic feature in PNP and other nucleoside phosphorylases and hydrolases (*37*).

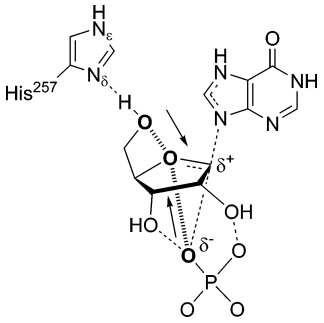

FIGURE 2: Proposed role of His^{257} in formation of the transition state, featuring dynamic compression of the O5′−O4′−O_P oxygen stack. The oxygen stack is represented by hashed bonds connecting bolded atoms, and arrows indicate promoting vibrational modes. Dashed bonds represent hydrogen bonds or partial bonds. Dynamic motion in the enzyme active site pushes O5′ and the phosphate oxygen toward the ring oxygen, leading to increased electron density in the center of reactivity. This contributes electron density to weaken the N9−C1′ bond, enhances hypoxanthine's leaving group ability, and forms the developing ribooxacarbenium ion.

contribute to catalysis dynamically, with vibrational compression of the three oxygen atoms providing electron density that enhances the leaving group ability of the purine base through stabilization of the oxacarbenium-like transition state (Figure 2). We have also investigated the role of His^{257} through mutagenesis to evaluate the corresponding kinetic and structural impacts. X-ray crystal structures with bound ImmH and DADMe-ImmH, transition-state analogues for HsPNP, reveal distortion of the 5′-OH when H-bonding to this group is removed. The 5′-^{3}H *V/K* KIEs and BIEs on the native and mutant enzymes were determined to establish the relative contributions to catalysis provided by formation of the Michaelis complex and subsequent changes at the transition state.

MATERIALS AND METHODS

Site-Directed Mutagenesis. The PCR product for HsPNP was cloned into the pCR-T7/CT-TOPO vector (Invitrogen), using samples and methods described previously (*5*, *9*). The resulting plasmid was transformed into TOP10F′ chemically competent *Escherichia coli* cells (Invitrogen) and grown overnight on LB agar plates containing 100 μg/mL ampicillin. Plasmids isolated from positive transformants were characterized by restriction analysis using HindIII and XbaI (New England Biolabs). The sequence of the HsPNP gene, including a stop codon prior to the C-terminal histidine tag of the TOPO vector, was confirmed by automated DNA sequencing (Albert Einstein College of Medicine, Bronx, NY).

Mutants were prepared according to the protocol of the QuikChange site-directed mutagenesis kit (Stratagene). Oligonucleotide pairs that were used to introduce mutations into the forward and reverse directions are listed below, with the mutated nucleotides underlined. Primers used for the His257Gly mutant were 5′-CTGGAGAAGGCCAACGGTGAAGAAGTCTTAGCA-3′ (forward) and 5′-TGCTAAGACTTCTTCCACCGTTGGCCTTCTCCAG-3′ (reverse). Primers used for the His257Phe mutant were 5′-GCCTGGAGAAGGCCAACTTTGAAGAAGTCTTAGCAGCTG-3′ (forward) and 5′-CAGCTGCTAAGACTTCTTCAAAGTTGGCCTTCTCCAGGC-3′ (reverse). Primers used for the His257Asp mutant were 5′-CTGGAGAAGGCCAACGATGAAGAAGTCTTAGCAGC-3′ (forward) and 5′-GCTGCTAAGACTTCTTCATCGTTGGCCTTCTCCCAG-3′ (reverse). All mutations were confirmed by automated DNA sequencing.

Overexpression and Purification of PNP Mutants. The H257G and H257F recombinant plasmids were transformed into BL21Star(DE3) chemically competent *E. coli* (Invitrogen), and the His257Asp recombinant plasmid was transformed into BL21AI(DE3) competent cells (Invitrogen). Positive transformants from overnight incubation on LB agar plates containing 100 μg/mL ampicillin were used to inoculate 10 mL cultures grown overnight in LB containing 100 μg/mL ampicillin at 37 °C with shaking at 200 rpm.

The overnight cultures were poured into 1 L of LB medium containing 100 μg/mL ampicillin and grown at 37 °C with shaking at 225 rpm until an OD_{600} of 0.5−0.7 was reached. Cells were induced for overexpression for 3−4 h at 37 °C by addition of either 0.1% lactose (His257Gly and His257Phe) or 0.2% L-arabinose (His257Asp). Cells were harvested at 4000 rpm for 30 min and stored at 4 °C overnight. Cell pellets were resuspended in 5−6 mL of lysis buffer [50 mM Tris-HCl (pH 8.0) containing one Complete protease inhibitor cocktail tablet (Roche Applied Science) per 50 mL and ∼1 mg of DNase I] per gram of pellet weight and lysed by sonication (5 min at 20% duty cycle, power level 6, 400 Watts) on ice. The cell lysate was clarified by centrifugation at 18 000 rpm for 30 min.

The clarified cell lysate was loaded at 2 mL/min onto a 140 mL column of Q-Sepharose Fast Flow resin (Amersham), pre-equilibrated with buffer [50 mM Tris-HCl (pH 8.0)]. After being washed with 2 column volumes of buffer at 4.6 mL/min, the desired protein was eluted with a linear salt gradient (buffer containing 0−0.25 M NaCl, applied over 6 column volumes). Fractions containing the mutant enzyme were identified by SDS−PAGE, pooled, and concentrated by ultrafiltration with a 400 mL Amicon stirred cell [10 kDa molecular mass cutoff, Millipore], followed by a 15 mL centrifugal filter (10 kDa molecular mass cutoff, Millipore). The concentrated enzyme solution [approximately 20 mg/mL by A_{280}, assuming $\epsilon_{280} = 28\,830\ M^{-1}\ cm^{-1}$ (*10*)] was then rapidly frozen in liquid nitrogen and stored at −80 °C.

Purified proteins were found to be >95% pure by SDS−PAGE, and the presence of the correct amino acid substitutions was confirmed by electrospray ionization mass spectrometry: His257Gly, 32 061 Da (calcd 32 067 Da); His257Phe, 32 154 Da (calcd 32 157 Da); and His257Asp, 32 123 Da (calcd 32 125 Da).

Overexpression and Purification of Histidine-Tagged Wild-Type HsPNP. Native human PNP was expressed and purified as the N-terminal histidine-tagged fusion as previously described (*5*).

Crystallization. The HsPNP·DADMe-ImmH·SO_4 crystal complexes were prepared by hanging-drop vapor diffusion at 18 °C by mixing the protein solution (2 μL of a 20 mg/mL solution) containing DADMe-ImmH (1:1.5 stoichiometry) with an equal volume of the reservoir solution containing 100 mM sodium citrate (pH 5.0) and 1.4 M $(NH_4)_2SO_4$ (Hampton) and equilibrating against 1.0 mL of the reservoir solution. The HsPNP·ImmH·PO_4 crystal complexes were prepared by sitting-drop vapor diffusion by mixing the protein solution (1 μL of a 20 mg/mL solution) containing ImmH and PO_4 (each 1.5 stoichiometry with respect to protein) with an equal volume of the reservoir solution containing 100 mM NaOAc (pH 4.6) and 4.0 M NH_4OAc and equilibrating against 80 μL of the reservoir solution. Crystals appeared in 2 days and grew to the maximum size of 0.3 mm × 0.3 mm × 0.3 mm. Diffraction from the HsPNP mutant crystals is consistent with space group *R*32 ($a = b = 142$ Å, and $c = 166$ Å), with a monomer in the asymmetric unit ($V_m = 4.7$ Å^3/Da; 76% solvent content).

Data Collection and Structure Refinement. HsPNP·DADMe-ImmH·SO_4 mutant crystals were transferred to a cryoprotectant composed of crystallization solution containing 20% glycerol and flash-cooled at −178 °C. HsPNP·ImmH·PO_4 mutant crystals were flash-cooled without cryoprotection. X-ray diffraction data were collected at a wavelength of 1.1 Å on a Quantum 315 CCD detector using synchrotron radiation at beamline X29A at the Brookhaven National Synchrotron Light Source. Data were reduced using the HKL package (*11*). HsPNP mutants were crystallized in the same space group as the native apoprotein. The structures of the native HsPNP apo form cocrystallized with DADMe-ImmH (PDB entry 1RSZ)[2] or ImmH (PDB entry 1RR6) were used as starting models for the refinement using CNS (*12*) or REFMAC5 (*13*), respectively. Mutated side chains were built into the density map using O (*14*) and COOT (*15*). The final models with DADMe-ImmH include residues 3−284, DADMe-ImmH, and two sulfate ions for each monomer, while the final models with ImmH contained residues 1−286, one ImmH, and one phosphate for each monomer. The model exhibits good stereochemistry as determined by PROCHECK (*16*). The structures have been submitted to the Protein Data Bank as entries 2A0W, 2A0X, and 2A0Y for His257Gly, His257Phe, and His257Asp, respectively, with DADMe-ImmH and 2OC9, 2ON6, and 2OC4, respectively, with ImmH. Data collection and structure refinement statistics are listed in Table 1.

Steady-State Kinetic Assays and Inhibition Studies. Catalytic activity was measured in 50 mM potassium phosphate (pH 7.4) at 25 °C, using a xanthine oxidase-coupled assay, as previously described (*17*), but with the inclusion of 5.0 mM dithiothreitol. The molar extinction coefficient for uric acid formation at 293 nm was taken to be 12 900 M^{-1} cm^{-1} (*18*). Histidine-tagged native and untagged mutant protein concentrations were determined by the absorbance at 280 nm using extinction coefficients of 31 650 and 30 160 M^{-1} cm^{-1}, respectively, which were calculated from their protein sequences (*19*). Inosine and inhibitor concentrations were determined spectrophotometrically using an ϵ_{260} of 7100 M^{-1} cm^{-1} (pH 6) (*20*) and an ϵ_{261} of 9540 M^{-1} cm^{-1} (pH 7) (*21*), respectively. Inhibitor dissociation constants for the phosphorolysis of inosine were based on initial and equilibrium reaction rate measurements with varied inhibitor concentrations (typically 2.0 nM to 2.0 μM). Reactions were performed in the presence of 5.0 mM dithiothreitol at fixed inosine concentrations of 1.0, 5.0, 5.0, and 15.0 mM for native HsPNP, His257Phe, His257Gly, and His257Asp, respectively. Reactions were initiated by the addition of PNP to final concentrations of 0.5−1.5 nM. In most cases, the inhibitor concentration was at least 10-fold greater than the enzyme concentration, as required for simple analysis of slow-onset tight-binding inhibition (*22*). When this condition could not be satisfied, corrections were made to compensate for the concentration of bound inhibitor (*23*).

Synthesis of [5′-^{3}H]Inosine and [5′-^{14}C]Inosine. To a solution of 500 μCi of [5′-^{3}H]uridine (33 nmol, 15 Ci/mmol, Moravek Biochemicals) in 50 μL of 10 mM Tris-HCl (pH 8.0) was added 1.0 μL of *E. coli* thymidine phosphorylase (1 unit, Sigma), 5.0 μL of HsPNP (∼11 units of a 32 mg/mL solution), and 1.0 μL of 1.0 mM hypoxanthine (Sigma). Note that *E. coli* TP accepts uridine as an alternative substrate. After incubation for 10 min at room temperature,

[2] C4″ is the carbon linking C4′ to N1′. The analogous atom in inosine is the ring oxygen, O4′.

Table 1: Data Collection and Structural Refinement Statistics

	His257Gly		His257Phe		His257Asp	
	DADMe, SO_4 (2A0W)	ImmH, PO_4 (2OC9)	DADMe, SO_4 (2A0X)	ImmH, PO_4 (2ON6)	DADMe, SO_4 (2A0Y)	ImmH, PO_4 (2OC4)
space group	*R*32	*R*32	*R*32	*R*32	*R*32	*R*32
unit cell (Å)						
a	141.881	142.441	141.764	143.011	142.467	143.386
b	141.881	142.441	141.764	143.011	142.467	143.386
c	166.399	168.765	166.172	168.324	166.029	168.457
			Data Collection			
resolution (Å)	50−2.28	30−2.60	50−2.28	30−2.50	50−2.28	30−2.60
no. of reflections						
total	267740	128876	265893	151918	262079	142541
unique	29413	19978	29401	21634	29445	20554
completeness (%)	99.9 (99.9)	97.2 (75.8)	99.9 (100)	94.5 (83.3)	99.9 (99.6)	99.3 (94.6)
R_{merge} (%)	4.6 (19.6)	6.9 (39.9)	6.2 (36.4)	6.6 (37.8)	5.1 (56.4)	7.1 (55.1)
			Structural Refinement			
R_{cryst} (%)	23.3	19.4	22.7	20.5	24.3	20.0
R_{free} (%)	25.4	24.0	25.1	24.6	26.7	24.7
no. of amino acids	282	284	282	286	282	286
no. of ligands	1 DADMe, 2 SO_4	1 ImmH, 1 PO_4	1 DADMe, 2 SO_4	1 ImmH, 1 PO_4	1 DADMe, 3 SO_4	1 ImmH, 1 PO_4
no. of waters	79	48	60	50	46	53
			Root-Mean-Square Deviation			
bonds (Å)	0.007	0.024	0.007	0.022	0.007	0.029
angles (deg)	1.33	2.2	1.33	2.14	1.31	2.62
			Ramachandran Plot			
most favored regions	89.5	87.6	90.8	88.7	87.9	84
additional allowed regions	10.1	10.7	8.8	10.5	11.7	13.9
generously allowed regions	0.0	1.3	0.0	0.4	0.0	1.7
disallowed regions	0.4	0.4	0.4	0.4	0.4	0.4

[5′-^{3}H]inosine was obtained in >98% purity by reverse-phase HPLC [5% methanol in 50 mM ammonium formate (pH 4.0) at 1 mL/min] using an analytical C18 column (Deltapak, Waters). The specific radioactivity of the starting material suggests it is a mixture of 5′-*R* and 5′-*S* monolabeled epimers. [5′-^{14}C]Inosine was prepared from [6-^{14}C]glucose as previously described (*5*).

Kinetic Isotope Effect Measurements. KIEs were determined as described by Lewandowicz and Schramm (*5*). [5′-^{3}H]Inosine and [5′-^{14}C]inosine were mixed at a ratio of 3:1 and subjected to arsenolysis using 50 mM Tris-HCl (pH 7.5), 50 mM Na_2HAsO_4 (Sigma), 250 μM carrier inosine, and HsPNP. Reactions, monitored by reverse-phase HPLC equipped with a photodiode array detector, were allowed to proceed until approximately 30% conversion. A one-third volume aliquot was removed and allowed to react to 100% completion. The remainder was divided into two equal volumes and quenched by application to charcoal spin columns (100 mg of activated charcoal in a Qiagen DNA purification spin column, previously washed with 1 mL of 10 mM D-ribose in 10% ethanol). The labeled ribose was eluted with 5 × 0.5 mL of 10 mM D-ribose in 10% ethanol, mixed with 7 mL of scintillation fluid (National Diagnostics Liquiscint), and counted for at least five cycles of 10 min each.

The count rate was averaged over all cycles, and the ^{3}H and ^{14}C emissions were separated according to the spectra of standard ^{14}C samples in identical matrices according to eqs 1 and 2

$$\text{cpm}(^3\text{H}) = \text{cpm}_{\text{channelA}} - \text{cpm}_{\text{channelB}} \times (^{14}\text{C channel ratio}) \quad (1)$$

$$\text{cpm}(^{14}\text{C}) = \text{cpm}_{\text{channelB}} + \text{cpm}_{\text{channelB}} \times (^{14}\text{C channel ratio}) \quad (2)$$

where (^{14}C channel ratio) is the ratio of ^{14}C counts in channels A and B for a control compound, [1-^{14}C]glucose. The spectral windows are set such that no counts from ^{3}H appear in channel B. The ratios of ^{3}H to ^{14}C were determined for both the 30% reactions and the 100% reaction, and the KIEs, adjusted to 0% reaction, were calculated according to eq 3

$$\text{KIE} = \frac{\ln(1-f)}{\ln\left(1 - f\frac{R_f}{R_o}\right)} \quad (3)$$

where *f* is the fraction of reaction progress as determined by HPLC and R_f and R_o are the ratios of heavy to light isotope after partial and complete reaction, respectively. The forward commitment factor for HsPNP of 0.147 was previously determined (*5*).

Equilibrium Binding Isotope Effect Measurements. BIEs were determined as described by Lewis and Schramm using the ultrafiltration method (*24*, *25*). To a solution of 50 mM Tris-HCl (pH 7.4), 500 mM ammonium sulfate, and 16−18 μM inosine (>5:1 [5′-^{3}H]inosine:[5′-^{14}C]inosine ratio by disintegrations per minute) was added 18−20 μM HsPNP to a final volume of 325 μL. Three 100 μL aliquots were removed and added to the upper wells of the ultrafiltration apparatus, and 22 psi N_2 was applied for 60−90 min or until approximately half of the solution had passed through the dialysis membrane (10 kDa molecular mass retention limit) into the lower well. From both upper and lower wells, 25 μL of solution was sampled using a Hamilton syringe and added to 1 mL of water in a scintillation vial. Ten

Table 2: Steady-State Kinetic Parameters of HsPNP and His[257] Mutants

	K_m (μM)		k_{cat} (s^{-1})		k_{cat}/K_m (M^{-1} s^{-1})	
enzyme	value	*x*-fold change	value	*x*-fold change	value	*x*-fold change
native PNP[a]	40	1	56	1	1.4×10^6	1
His257Ala[a]	210	5	16	4	7×10^4	20
His257Phe	320 ± 12	8	6.55 ± 0.07	9	$(2.05 \pm 0.10) \times 10^4$	68
His257Gly	750 ± 60	19	1.75 ± 0.04	32	$(2.3 \pm 0.2) \times 10^3$	610
His257Asp	1350 ± 130	34	1.30 ± 0.05	41	$(9.6 \pm 1.3) \times 10^2$	1460

[a] Values obtained from ref *27*.

milliliters of scintillation fluid (National Diagnostics Liquiscint) was added, and the samples were counted for at least five cycles of 5 min each.

Spectral deconvolution of ^{3}H and ^{14}C was performed as described previously using a ^{14}C standard in a matrix identical to the BIE samples. The BIE was then calculated as the quotient of the ratio of ^{14}C to ^{3}H bound to the enzyme (R_b) and free in solution (R_f). R_b was determined according to eq 4:

$$R_b = \left(\frac{1}{1-f}\right)R_m - \left(\frac{f}{1-f}\right)R_f \quad (4)$$

where f is the fraction of substrate unbound in the upper well, which is taken as the ratio of ^{3}H below the membrane to that above, R_m is the ^{14}C:^{3}H ratio above the membrane, R_f is the ratio below the membrane, and R_b is the isotopic ratio of bound substrate.

Commitment to Catalysis. The isotope trapping method, similar to previously reported methods, was used to determine the commitment to catalysis (*4*, *5*). A pulse solution containing 50 mM Tris-HCl (pH 7.4), 260 μM [5′-^{14}C]inosine (ca. 10^5 cpm), and 30 μM His257Phe, 200 μM His257Gly, or 200 μM His257Asp was prepared and allowed to equilibrate at room temperature for 2 min. Ten microliters of this solution was then added to 200 μL of a chase solution containing 50 mM Tris-HCl (pH 7.4), 10 mM unlabeled inosine, and varying concentrations of sodium arsenate (from 1 μM to 100 mM). After approximately 6 s, the reaction was quenched by the addition of 50 μL of 1 M HCl. [5′-^{14}C]Ribose generated in the reaction was isolated by passing the mixture through charcoal columns (~150 mg of a 1:6 charcoal/cellulose mixture), preequilibrated with 20 mM ribose in 10% EtOH, and eluted with 2.75 mL of this solution. Seven milliliters of scintillation fluid was added, and the samples were counted for 1 min each. Controls measured the amount of ribose formed under the same conditions but either without enzyme or without arsenate. The forward commitment factor was determined by plotting [^{14}C]ribose/[^{14}C]inosine$_{released}$ against [AsO_4], where [^{14}C]-inosine$_{released}$ is the amount of inosine in the pulse solution not converted to ribose, given by eq 5:

$$[\text{Ino}]_{released} = \frac{[\text{Ino}]_p}{[\text{Ino}]_p + K_m}[\text{E}] - [\text{Rib}] \quad (5)$$

where $[\text{Ino}]_p$ is the total inosine in the pulse solution and K_m and [E] are the Michaelis constant and enzyme concentration for the mutant protein, respectively.

RESULTS AND DISCUSSION

To examine the contribution of His[257] to the unusually large 5′-^{3}H kinetic isotope effect observed in the PNP reaction and thereby assess its importance in binding and catalysis, this residue was mutated individually to glycine, phenylalanine, and aspartate. The His257Gly mutant was expected to eliminate bonding of hydrogen to the 5′-hydroxyl group of the substrate and to reduce the steric effects in its immediate proximity, possibly allowing it to rotate with less restriction. The His257Phe mutant would also remove hydrogen-bonding to the 5′-hydroxyl group but would retain steric bulk and hydrophobicity in this region of the active site. Finally, the His257Asp mutant would retain the possibility of H-bonding to the 5′-hydroxyl group while introducing only a minor decrease in size. These mutants were tested for their catalytic and structural properties, as well as their isotopic discrimination.

Steady-State Kinetics of His[257] Mutants. The effects of His[257] mutation on the steady-state kinetics of inosine phosphorolysis were determined (Table 2), and all three mutants exhibited compromised catalysis in K_m (inosine), k_{cat}, and k_{cat}/K_m. In comparison to the native enzyme, His257Phe gave an 8-fold increase in K_m and a 9-fold decrease in k_{cat}. As this mutant lacks H-bonding ability yet retains significant catalytic activity, it is clear that the H-bond between His[257] and the 5′-hydroxyl of inosine is not essential. This notion is further supported by the observation that 5′-deoxyinosine is a substrate for PNP (*26*). The kinetic values of His257Phe are similar to those obtained by Ealick and co-workers for His257Ala (Table 2) (*27*). Therefore, it appears that PNP has some tolerance for hydrophobic side chain substitutions at this position, likely due to the existence of hydrophobic neighboring residues within the ribose-binding cleft, including Val260, Leu261, and Phe200, as well as Phe159 from the adjacent monomer.

Removal of the side chain on residue 257, as in the His257Gly mutant, results in a more pronounced catalytic impairment, with 19- and 32-fold changes in K_m and k_{cat}, respectively. The resulting 610-fold decrease in catalytic efficiency (k_{cat}/K_m) compared to that of native HsPNP is likely due to the elimination of stabilizing interactions either with substrate via H-bonding or with neighboring residues via hydrophobic packing.

Intriguingly, His257Asp, the mutant that conserved the 5′-OH H-bond with the native enzyme, suffered the greatest impact on catalysis. The increase in K_m from 40 μM to 1.35 mM, combined with the 41-fold decrease in k_{cat}, resulted in a drop in catalytic efficiency by a factor of 1400. The substitution of a carboxyl group for the imidazole side chain of histidine introduces a functional group with a lower pK_a. As a result, the electrostatic environment surrounding the 5′-OH is made more negative, and the H-bond strength between this hydroxyl group and residue 257 may have been altered. That the negative charge in the active site is not tolerated well is supported by the observation that activity

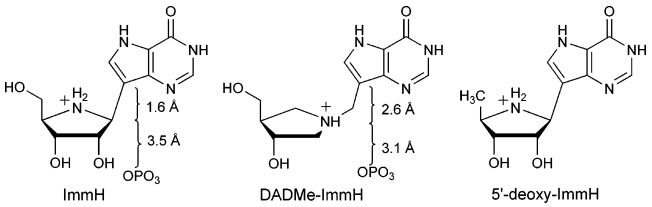

FIGURE 3: Transition-state analogue inhibitors of HsPNP. ImmH and DADMe-ImmH are shown with their respective C1′−C9 (N1′−C9) and C1′−O_P distances. Inhibition by 5′-deoxy-ImmH was also tested in this study for comparison with the His^{257} mutants.

in this mutant increases at more acidic pH values (maximal at pH 6.3), where the neutral form of the side chain is more favorable.

Inhibition of His^{257} Mutants by Transition-State Analogues. Immucillin-H (ImmH; Figure 3) and DADMe-Immucillin-H (DADMe-ImmH) are tight-binding transition-state analogue inhibitors of HsPNP, exhibiting slow-onset inhibition with dissociation constants (K_i*) of 58 and 11 pM, respectively. The greater affinity for DADMe-ImmH is attributed to placement of the cationic charge at the anomeric position and to increased separation between the sugar ring and leaving group (2.6 Å vs 1.6 Å for ImmH), characteristics which allow DADMe-ImmH to more closely resemble HsPNP's dissociative oxacarbenium ion transition state (Figure 1b) (*28*). When DADMe-ImmH was tested with each of the His^{257} mutants, it was found to give K_i* values between 270 and 950 pM (Table 3). After we account for differences in K_m among the variants, this yields K_m/K_i values from 337 000 to 2 800 000, all within a factor of 11 of the native value of 3 700 000. Thus, DADMe-ImmH binds nearly as tightly to the mutants as to native HsPNP. In contrast, differences of as much as 370-fold in K_m/K_i were observed with ImmH (Table 3). Simple competitive inhibition occurred with these mutants with ImmH, in contrast to the slow-onset inhibition kinetics exhibited with the native enzyme (Figure 4). This finding reveals the importance of His^{257} in the early progress toward the transition state, which is mimicked by the molecular electrostatic structure of ImmH. As mentioned earlier, the H-bond to His^{257} has been proposed to steer the 5′-OH into alignment with O4′ and the oxygen of the approaching nucleophile. In the later stages of the reaction coordinate, which is better mimicked by DADMe-ImmH, this residue apparently plays a diminished role, and interactions at the reaction center become more significant. Specifically, the ion pair between sulfate (a mimic of the phosphate anion) and the DADMe-ImmH cation is more favorable than that with ImmH (N−O distances of 3.1 and 3.7 Å, respectively).

To verify the importance of the interaction between His^{257} and the 5′-hydroxyl for tight-binding inhibition with ImmH, 5′-deoxy-ImmH (Figure 3) was tested with HsPNP and the mutant proteins. This inhibitor bound to native PNP with 345-fold less affinity (K_i = 20 nM) than ImmH and did not exhibit slow-onset inhibition (Table 3). However, the native K_m/K_i of 2000 for 5′-deoxy-ImmH is the same as that for His257Phe with ImmH. Intriguingly, the mutant proteins bound 5′-deoxy-ImmH up to 9-fold better than ImmH, perhaps reflecting favorable hydrophobic interactions with the 5′-methyl group.

Structures of His^{257} Mutants Complexed with DADMe-ImmH and ImmH. Each His^{257} mutant was crystallized in the presence of DADMe-ImmH and sulfate, a mimic of the phosphate nucleophile. Structures of these mutants, obtained at 2.3 Å resolution, were determined by molecular replacement using the previously obtained structure of the native protein.[3] All three are highly similar to native HsPNP, with rms deviations of 0.14−0.17 Å in the backbone α-carbons, and with only small differences in the active site (Figure 5a). In mutant and native PNP structures with DADMe-ImmH, the orientation of the 5′-OH group of the bound transition-state analogue is unchanged. As previously observed with the homologous PNP from *Mycobacterium tuberculosis* (*29*), the 60° O5′−C5′−C4′−C4″ dihedral angle[2] of DADMe-ImmH positions the 5′-OH group in a *syn* orientation with respect to the ring, thereby placing O5′ within 3.1 Å of C4″ (Figure 5b). This angle is conserved even in the His257Gly and His257Phe mutants, where no H-bond to O5′ is apparent. Similarly, this 60° dihedral angle is found in the structure of native HsPNP complexed with inosine (*30*), indicating that the orientation of the 5′-OH group is the same for bound inosine and DADMe-ImmH. The invariant dihedral angle in these bound ligands suggests that the orientation of the hydroxyl may be a preferred geometry for these molecules and may not be altered by the surrounding protein environment. This notion is supported by structural studies of inosine and other nucleosides, in which a *syn* conformation has been found to be statistically predominant for the molecule free in solution (*31*−*35*); however, the energetic barrier to full rotation at this position of inosine is estimated to be less than 9 kcal/mol in water, which is similar in magnitude to the barrier governing cyclohexane chair flipping (*36*).

The His^{257} mutants were also crystallized with ImmH and phosphate, and the resulting structures were determined by molecular replacement with the native structure.[3] In contrast to the case with DADMe-ImmH, the mutant complexes bind ImmH in differing orientations (Figure 6a). The ImmH-bound His257Gly complex did not differ significantly from the native form (Figure 6b), though the O5′−C5′−C4′−N4′ dihedral angle closed slightly from 59° to 57° (Figure 7). The His257Phe mutant was found to bind ImmH in a poorly ordered manner (Figure 6d). Electron density was absent for the 5′-hydroxyl group, and the inhibitor could be adequately modeled with the iminoribitol moiety rotated such that the 5′-hydroxyl points toward the phosphate molecule. Additionally, whereas the phenyl ring of Phe^{257} was shifted away from DADMe-ImmH (pink in Figure 6d), it was found to have moved closer to ImmH (blue in Figure 6d). The His257Asp mutant (Figure 6c), though maintaining the overall protein structure, greatly altered the orientation of the 5′-hydroxyl, decreasing the dihedral angle to 14° (Figure 7). This places O5′ directly above N4′ in a nearly eclipsed geometry reminiscent of the hypothetical oxygen stack. The aspartate residue in this mutant may have polarized the 5′-hydroxyl, to increase its electronegativity and promote its interaction with the positively charged N4′. When the structural changes imposed on ImmH due to mutation of His^{257} are taken in light of the poor binding of this transition-state analogue observed in the inhibition

[3] W. Shi, A. Lewandowicz, P. C. Tyler, R. H. Furneaux, S. C. Almo, and V. L. Schramm, unpublished results.

Table 3: Dissociation Constants of Transition-State Analogues with HsPNP and His^{257} Mutants

	DADMe-ImmH			ImmH				5′-deoxy-ImmH		
		K_m/K_i				K_m/K_i			K_m/K_i	
enzyme	K_i*[a] (pM)	value	*x*-fold change	K_i (nM)	K_i* (pM)	value	*x*-fold change	K_i[b] (nM)	value	*x*-fold change
native	10.7 ± 1.1	3 700 000	1	*a*	57.9 ± 1.5	690000	1	20.0 ± 0.9	2000	1
His257Phe	950 ± 60	337 000	11	172 ± 16	*b*	1860	370	19.8 ± 1.0	16200	8
His257Gly	270 ± 20	2 800 000	1	11.0 ± 0.9	*b*	68100	10	7.7 ± 0.6	97000	93
His257Asp	900 ± 100	1 500 000	2	86 ± 7	*b*	15700	45	54 ± 3	25000	12

[a] The weak inhibition phase (K_i) was observed but too short to quantitate, so only the slow-onset, tight-binding phase (K_i*) is reported. [b] No slow-onset phase was observed.

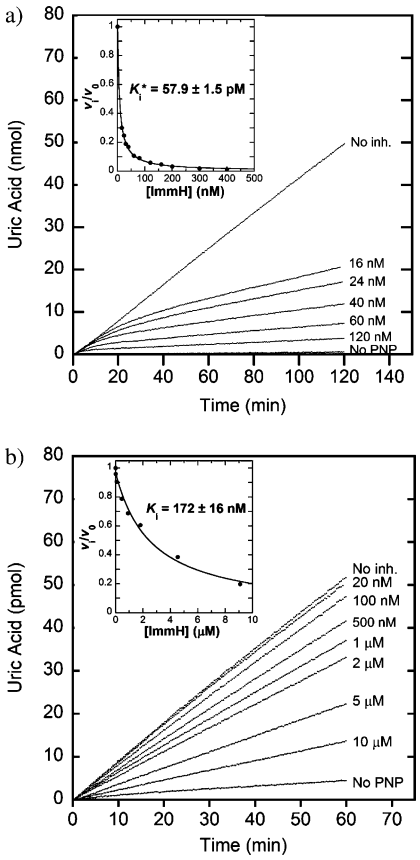

FIGURE 4: Inhibition of native HsPNP and His257Phe by ImmH. (a) Slow-onset inhibition measured for native HsPNP in the presence of ImmH at the indicated concentrations. Hypoxanthine formation is monitored by conversion to uric acid by a xanthine oxidase-coupled assay. In the inset, the rate during incubation for 100−120 min with inhibitor (v_i) relative to that of an uninhibited sample (v_0) is plotted against the inhibitor concentration to calculate the dissociation constant, K_i*. Panel b shows the corresponding plots for His257Phe with ImmH.

studies, it is clear that His^{257} is important for the enzyme as the reaction approaches the transition state.

Intrinsic Kinetic Isotope Effects from V/K Kinetic Isotope Effects and Binding Isotope Effects. Kinetic isotope effects have been useful in the elucidation of transition-state structures for *N*-ribosyltransferase reactions (*37*, *38*). Although *V/K* KIEs are used in determining these structures, they do not differentiate isotopically sensitive binding events from chemistry at the transition state. Binding isotope effects are usually small and are often ignored, especially when large isotope effects are being considered. However, when secondary deuterium or tritium isotope effects are used to establish a transition-state structure, BIEs are valuable for distinguishing bond distortion and polarization upon binding from that occurring in the transition state (*39*).

The importance of distinguishing BIEs from *V/K* KIEs is particularly applicable for remote isotope effects. Although KIEs are not expected for atoms that are several bonds removed from the reactive center, remote 5′-^{3}H KIEs have been measured in several *N*-ribosyltransferases and hydrolases, including TP (*4*), pertussis toxin, cholera toxin, diphtheria toxin (*40*−*43*), nucleoside hydrolase (*44*), and mammalian PNPs (*5*, *45*). The *V/K* 5′-^{3}H KIE of 5.4% previously determined for HsPNP was calculated as an "intrinsic" KIE of 6.2% with the assumption that there are no isotopically sensitive steps aside from the chemical event. This large KIE has been attributed to distortions in the vibrational modes of the C5′−H bonds that occur during the progression from the unbound substrate to the transition state (*5*). The BIE analysis of TP by Birck and Schramm (*2*, *4*), however, highlights the importance of determining the relative contributions to the *V/K* KIE that are attributable to isotopic discrimination during formation of the Michaelis complex.

The intrinsic KIE from the chemical nature of the transition state is a function of the *V/K* KIE and the BIE, both of which can be determined experimentally using appropriate competitive experiments with isotopically labeled substrates (Figure 1). For this scheme, assuming the chemical step is irreversible (i.e., k_4 and reverse commitment, $C_r = 0$), the *V/K* KIE, symbolized as $^T(V/K)$, is related to the equilibrium BIE ($^TK_{eq}$) and the intrinsic KIE ($^Tk_3$) by eq 6 (*39*, *46*):

$$^T(V/K) = \frac{^TK_{eq}\,^Tk_3 + ^Tk_1C_f}{1 + C_f} \quad (6)$$

where $^Tk_1$ is the intrinsic KIE for binding and C_f is the forward commitment to catalysis, defined as k_3/k_2. In cases where C_f is low, the $^Tk_1C_f$ term in eq 6 can be approximated within experimental error as C_f,[4] yielding eq 7:

$$^T(V/K) = \frac{^TK_{eq}\,^Tk_3 + C_f}{1 + C_f} \quad (7)$$

[4] The unprecedented measurement of a kinetic isotope effect on binding would not significantly change the results and interpretations of this study. A $^Tk_1$ similar in magnitude to the BIEs would result in calculated $^Tk_3$ values of 1.044, 0.962, 0.845, and 1.070 for native PNP, His257Phe, His257Gly, and His257Asp, respectively, corresponding to changes of 0.2, 0.6, 1.4, and 0.1%, respectively. Thus, for all but His257Gly, which has the largest forward commitment, the assumption of a unity $^Tk_1$ is within experimental error.

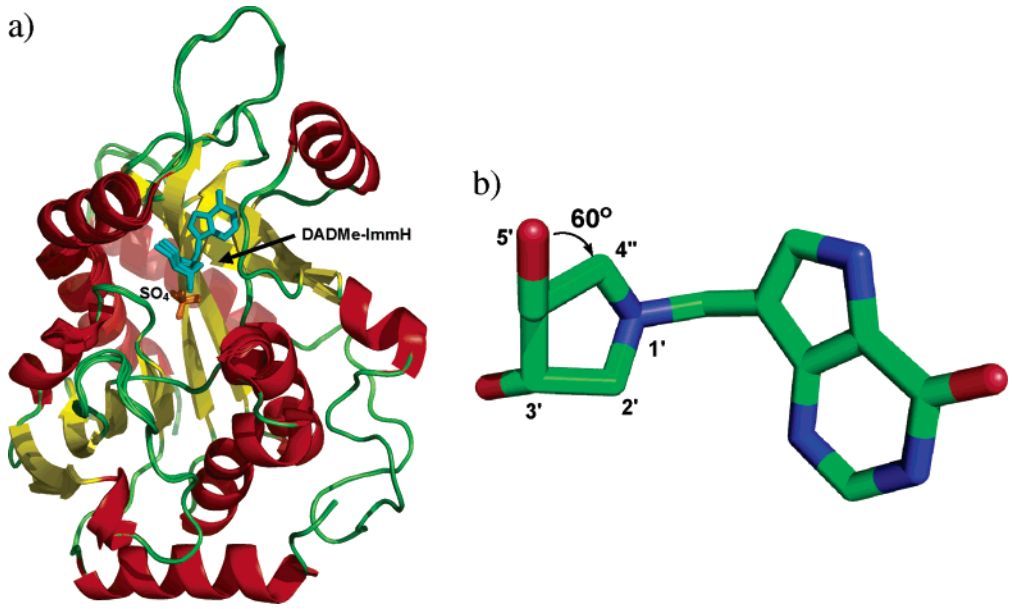

FIGURE 5: Crystal structures of HsPNP and His^{257} mutants complexed with DADMe-ImmH and SO_4. (a) The superposition of the monomeric structures of the four HsPNP His^{257} variants reveals very few differences in the position of DADMe-ImmH (cyan) at the active sites. Secondary structural elements are colored red for α-helices, yellow for *β*-sheets, and green for random coils. (b) Dihedral angle between the O5′−C5′ and C4′−C4″ bonds in PNP-bound DADMe-ImmH. The model is viewed down the C5′−C4′ bond.

Thus, the intrinsic KIE on the chemical step of interest is obtained through the determination of the *V*/*K* KIE, the BIE, and the forward commitment.

5′-^{3}H Binding Isotope Effects and Kinetic Isotope Effects on HsPNP. The competitive binding of [5′-^{3}H]inosine and [5′-^{14}C]inosine to HsPNP was assessed in the presence of sulfate, a phosphate analogue that precludes phosphorolysis. Normal BIEs of 2% were determined for the native enzyme, His257Phe, and His257Gly (Table 4), indicating that [5′-^{1}H]inosine binds more tightly than [5′-^{3}H]inosine, and therefore, the vibrational environment of the 5′-hydrogen(s) has become less constrained in the Michaelis complex. In contrast, a small but inverse BIE of −2% was found for His257Asp, indicating an increased constraint upon the 5′-hydrogen(s) such that the tritiated substrate is slightly preferred in the Michaelis complex. Note that because the labeled substrate exists as a mixture of (*R*)- and (*S*)-[5′-^{3}H]-inosine, the observed isotope effects are averages of each stereoisomer, and therefore, their origin cannot be assigned to a single molecular orbital.

Competitive *V*/*K* KIEs and forward commitment factors were measured for the three His^{257} mutants (Table 4), as performed previously with the native enzyme (*5*). The intrinsic KIEs for all four enzymes were calculated from the *V*/*K* KIEs and BIEs by eq 7. Native HsPNP and the His257Asp mutant gave large normal intrinsic KIEs of 4.6 and 6.9%, respectively, whereas His257Phe and His257Gly exhibited inverse isotope effects of −3.2 and −14.1%, respectively. These results indicate that although the native enzyme retains its preference for the lighter isotopologue throughout catalysis, the mutants undergo a reversal of preference during progress from the Michaelis complex to the transition state.

Although the origin of the 5′-^{3}H isotope effect may be more complicated than what can be explained by present theory, two features at this position have been demonstrated in model systems to contribute to remote isotope effects. These factors are (1) polarization of the 5′-hydroxyl group and (2) its orientation relative to one of the C5′−H *σ**-orbitals, both of which cause significant changes in the C5′−H bond length, as illustrated by Lewis and Schramm through computational analysis of a 2-propanol/formate model (Figure 8a) (*24*). They demonstrated that as the H-bonding partners are brought closer together, the O−H bond becomes more polarized, resulting in a decreased bond order in the adjacent C−H bond. This causes a normal isotope effect, the magnitude of which increases as the distance between H-bonding partners decreases. Lewis and Schramm further showed that alteration of the conformational orientation of the hydroxyl group (H−C−O−H torsional angle in 2-propanol) causes significant changes in C−H bond stretching and bending force constants (Figure 8b). Depending on the dihedral angle, the oxygen's lone pair orbitals may hyperconjugate with the C−H antibonding orbitals, giving rise to normal isotope effects, or they may overlap poorly, leading to inverse isotope effects. Thus, contributions from polarization and hydroxyl orientation may work in concert or opposition to yield normal or inverse BIEs and KIEs.

Although the 1.5% BIE found with native HsPNP can be explained by the H-bond to His^{257}, this interaction cannot be invoked for the BIEs of the mutant proteins. His257Gly and His257Phe lack H-bond potential for the 5′-hydroxyl, and although His257Asp retains H-bond capability, it exhibits an inverse BIE. Therefore, the orientation of the 5′-hydroxyl must be a dominant factor in the Michaelis complex. Since the BIEs of native HsPNP, His257Gly, and His257Phe are similar, the dihedral angle between the 5′-H_R or 5′-H_S and the O5′−H bond is proposed to be similar in their respective Michaelis complexes. The generation of the BIE involves an increased level of hyperconjugation relative to that of unbound inosine in solution. In the case of His257Asp, however, bond polarization is likely the dominant factor, as supported by the ImmH structural data. This would result in

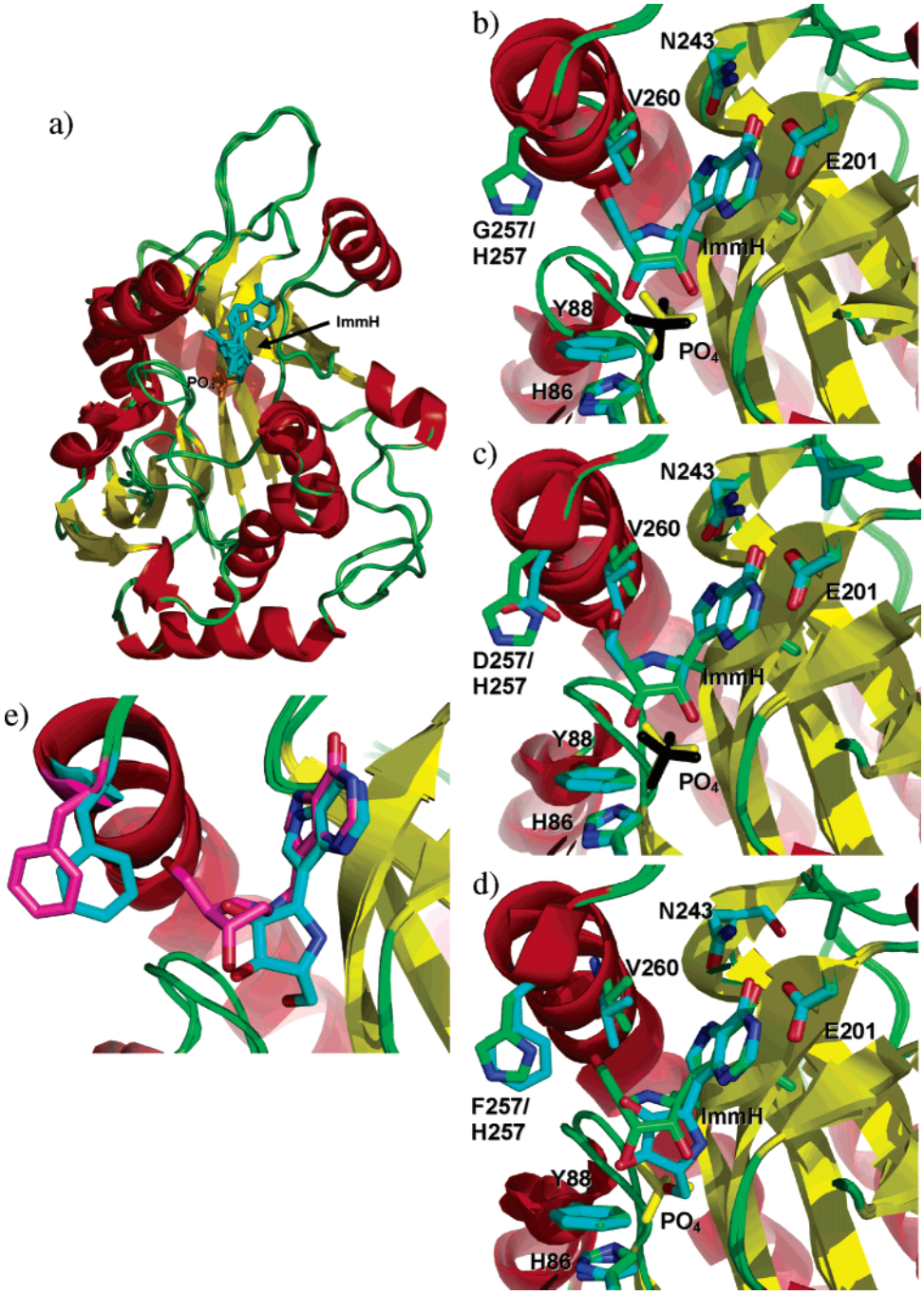

FIGURE 6: Crystal structures of HsPNP and His[257] mutants complexed with ImmH and PO_4. (a) The superposition of the monomeric structures of the four HsPNP His[257] variants reveals differences in the orientation of ImmH (cyan) at the active sites. Secondary structure elements are colored red for α-helices, yellow for *β*-sheets, and green for random coils. The overlays of the active site regions of native HsPNP and (b) His257Gly, (c) His257Asp, and (d) His257Phe show small changes in the region surrounding the 5′-hydroxyl of the bound inhibitor. Side chains of selected active site residues within 3.2 Å of ImmH have been included. Carbon atoms of these side chains and of the inhibitor are colored green for native HsPNP and cyan for the mutant proteins. Phosphate molecules bound to the native and mutant variants are colored yellow and black, respectively. Water molecules have been excluded for clarity. (e) Superposition of His257Phe·DADMe-ImmH·SO_4 (magenta) and His257Phe·ImmH·PO_4 (cyan) complexes showing the differences in the positions of Phe[257] and the ligand. For the Phe mutant in panels d and e, only one of the two most probable orientations of ImmH has been illustrated; in this case, the phosphate ligand cannot be conclusively located.

poorer n → σ^* orbital overlap and the generation of an inverse BIE.

The intrinsic KIEs were larger than the corresponding BIEs, indicating that the *V*/*K* KIEs are dominated by transition-state chemistry, rather than binding of inosine. This finding is in contrast to TP, where the BIE was found to be equal to the *V*/*K* KIE (*2*). The difference may be related to the S_N1-like mechanism involving an oxacarbenium ion transition state of PNP, while the transition state of TP has S_N2 character. These mechanistic distinctions will result in positional and H-bonding environmental differences for the 5′-hydroxyl.

The intrinsic KIEs for HsPNP and the His[257] mutants reveal a dichotomy where enzyme variants capable of H-bonding to the 5′-hydroxyl, native HsPNP and His257Asp, give rise to normal KIEs, while those incapable of H-

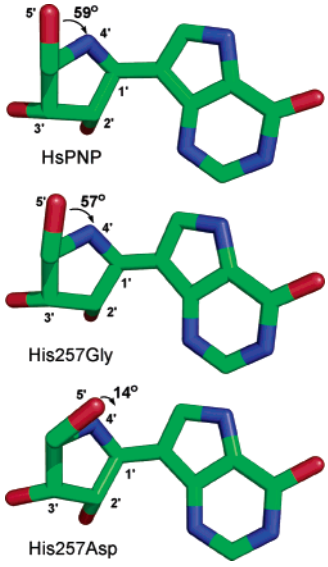

FIGURE 7: Dihedral angle between the O5′−C5′ and C4′−N4′ bonds of ImmH bound to native HsPNP, His257Gly, and His257Asp. The models are viewed down the C5′−C4′ bond.

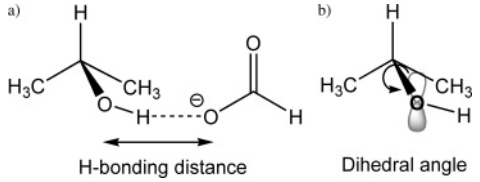

FIGURE 8: 2-Propanol/formate model of Lewis and Schramm (*24*, *39*) for estimating the effects of (a) hydrogen bond distance and (b) dihedral angle rotation on the binding isotope effects. Shorter H-bonds cause an increased level of polarization, which enhances hyperconjugation between the oxygen's lone pair electrons and the antibonding orbital of the adjacent C−H bond. Dihedral angles that increase or decrease the degree of overlap of the oxygen's lone pair orbital with the σ*-orbital give rise to an increased or decreased level of hyperconjugation, respectively, and therefore may result in either normal or inverse isotope effects.

bonding, His257Gly and His257Phe, result in inverse KIEs. This observation suggests that polarization of the O5′−H bond may dominate over other factors. In particular, the dihedral angle of DADMe-ImmH bound at the catalytic site of native HsPNP and all mutants is the same, but the differences in BIEs establish differences in the vibrational environment and/or bond polarization. Substitution of an aspartate residue, a stronger H-bond acceptor than histidine, results in a larger intrinsic KIE and strengthens this proposal. The inverse intrinsic KIEs observed for the His257Gly and His257Phe mutants can be rationalized by the combined effect of the lack of polarization due to the absence of H-bonding as well as a decrease in electron density at O5′ during formation of the transition state. As hypothesized in the dynamic mechanism of PNP catalysis (Figure 2), O5′ is moved toward O4′ to form an oxygen stack that destabilizes electrons on O4′ and leads to the developing oxacarbenium ion. This donation of electron density from the lone pair electrons causes a further decrease in the level of hyperconjugation to the C5′−H σ*-orbitals, resulting in an inverse KIE.

Table 4: 5′-^{3}H Kinetic Isotope Effect and Binding Isotope Effect Data

enzyme	*V*/*K* KIE	BIE	C_f	intrinsic KIE
native PNP	1.054 ± 0.002[a]	1.015 ± 0.003	0.147[a]	1.046 ± 0.004
His257Phe	0.992 ± 0.003	1.022 ± 0.004	0.301 ± 0.010	0.968 ± 0.005
His257Gly	0.925 ± 0.005	1.024 ± 0.006	0.600 ± 0.021	0.859 ± 0.007
His257Asp	1.046 ± 0.004	0.980 ± 0.005	0.042 ± 0.002	1.069 ± 0.007

[a] Value reported in ref *5*.

CONCLUSIONS

Detailed atomic information of enzymatic transition-state structures is important for understanding the reaction mechanism and for the development of transition-state analogue inhibitors. Investigation of the interactions between His^{257} and the 5′-hydroxyl in HsPNP through mutagenesis and subsequent kinetic and structural studies has revealed new information about the remote contributions to catalysis. Further, combined analysis of BIEs and KIEs has enabled the resolution of distortion in the Michaelis complex from intrinsic isotope effects as a result of transition-state chemistry. Together, these experiments have provided a more detailed understanding of the enzymatic mechanism (Figure 9). The enzyme approaches the transition state through His^{257}-directed dynamic movement of the 5′-hydroxyl over O4′ which promotes the departure of hypoxanthine by the movement of electrons toward C1′. Approach to the dissociative transition state initially proceeds through a point at which the relative electron deficiency of the incipient oxacarbenium ion is localized more at O4′, and the hypoxanthine is closer to the ribose than the phosphate nucleophile. As the phosphate−ribose distance decreases and the hypoxanthine−ribose distance increases, there is a shift in the positive charge localization to C1′. These two stages of transition-state development are analogous to ImmH and DADMe-ImmH, which are known to mimic early and later

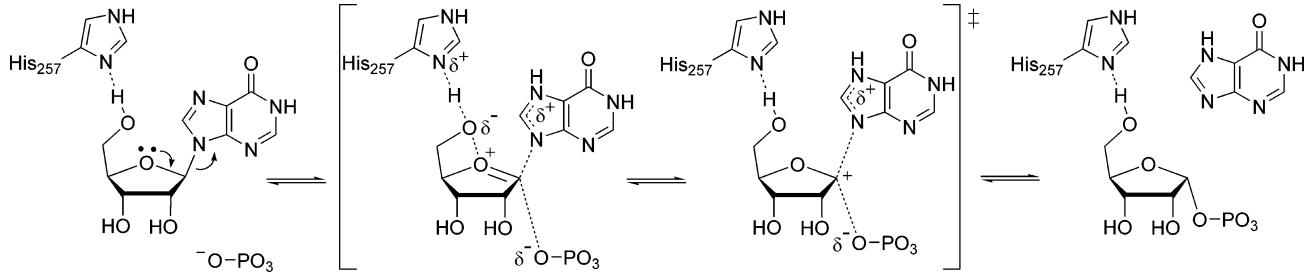

FIGURE 9: Mechanism of the HsPNP reaction illustrating the role of His^{257}. The H-bond between N_δ of His^{257} and the 5′-hydroxyl polarizes O5′, which is steered toward O4′. This electron density loosens the 4′-oxygen's lone pair electrons, which interact with the antibonding orbital of the C1′−N9 bond. Further along the reaction coordinate, as the bond to the leaving group is largely broken, significant positive charge density is localized at C1′. Formation of a bond to the nucleophile completes the phosphorolysis reaction. N7 of the leaving group has been depicted as being protonated at the transition state, as this has been demonstrated to be a common mechanistic feature in PNP and other nucleoside phosphorylases and hydrolases (*37*).

transition-state structures, respectively. These experiments expand on the nature of intrinsic KIEs and the transition state for PNP. The inhibitory characteristics of the transition-state analogues ImmH and DADMe-ImmH are better defined through these results.

ACKNOWLEDGMENT

The authors thank Drs. Peter Tyler, Richard Furneaux, and Gary B. Evans of Industrial Research, Ltd. (Lower Hutt, New Zealand), for the synthesis of ImmH and DADMe-ImmH, Dr. Andrzej Lewandowicz for the plasmid encoding native human PNP, and Dr. Suwipa Saen-Oon for computational analysis of the dihedral angles of inosine, and the staff at NSLS Brookhaven National Laboratory for technical assistance at beamline X29A.

SUPPORTING INFORMATION AVAILABLE

Calculation of the barrier to 5′-OH rotation in inosine and crystal structures of native and mutant PNPs complexed with DADMe-ImmH and SO_4 depicting active site details and closest contacts. This material is available free of charge via the Internet at http://pubs.acs.org.

REFERENCES

1. Northrop, D. B. (1981) The expression of isotope effects on enzyme-catalyzed reactions, *Annu. Rev. Biochem. 50*, 103−131.
2. Birck, M. R., and Schramm, V. L. (2004) Binding causes the remote [5′-^{3}H]thymidine kinetic isotope effect in human thymidine phosphorylase, *J. Am. Chem. Soc. 126*, 6882−6883.
3. LaReau, R. D., Wan, W., and Anderson, V. E. (1989) Isotope effects on binding of NAD^+ to lactate dehydrogenase, *Biochemistry 28*, 3619−3624.
4. Birck, M. R., and Schramm, V. L. (2004) Nucleophilic participation in the transition state for human thymidine phosphorylase, *J. Am. Chem. Soc. 126*, 2447−2453.
5. Lewandowicz, A., and Schramm, V. L. (2004) Transition state analysis for human and *Plasmodium falciparum* purine nucleoside phosphorylases, *Biochemistry 43*, 1458−1468.
6. Fedorov, A., Shi, W., Kicska, G., Fedorov, E., Tyler, P. C., Furneaux, R. H., Hanson, J. C., Gainsford, G. J., Larese, J. Z., Schramm, V. L., and Almo, S. C. (2001) Transition state structure of purine nucleoside phosphorylase and principles of atomic motion in enzymatic catalysis, *Biochemistry 40*, 853−860.
7. Pugmire, M. J., and Ealick, S. E. (2002) Structural analyses reveal two distinct families of nucleoside phosphorylases, *Biochem. J. 361*, 1−25.
8. Nunez, S., Antoniou, D., Schramm, V. L., and Schwartz, S. D. (2004) Promoting vibrations in human purine nucleoside phosphorylase. A molecular dynamics and hybrid quantum mechanical/molecular mechanical study, *J. Am. Chem. Soc. 126*, 15720−15729.
9. McIvor, R. S., Goddard, J. M., Simonsen, C. C., and Martin, D. W., Jr. (1985) Expression of a cDNA sequence encoding human purine nucleoside phosphorylase in rodent and human cells, *Mol. Cell. Biol. 5*, 1349−1357.
10. Stoeckler, J. D., Agarwal, R. P., Agarwal, K. C., Schmid, K., and Parks, R. E., Jr. (1978) Purine nucleoside phosphorylase from human erythrocytes: Physiocochemical properties of the crystalline enzyme, *Biochemistry 17*, 278−283.
11. Otwinowski, Z., and Minor, W. (1997) Processing of X-ray diffraction data collected in oscillation mode, *Methods Enzymol. 276*, 307−326.
12. Brunger, A. T., Adams, P. D., Clore, G. M., DeLano, W. L., Gros, P., Grosse-Kunstleve, R. W., Jiang, J. S., Kuszewski, J., Nilges, M., Pannu, N. S., Read, R. J., Rice, L. M., Simonson, T., and Warren, G. L. (1998) Crystallography & NMR system: A new software suite for macromolecular structure determination, *Acta Crystallogr. D54* (Part 5), 905−921.
13. Murshudov, G. N., Vagin, A. A., and Dodson, E. J. (1997) Refinement of macromolecular structures by the maximum-likelihood method, *Acta Crystallogr. D53*, 240−255.
14. Jones, T. A. (1985) Interactive computer graphics: FRODO, *Methods Enzymol. 115*, 157−171.
15. Emsley, P., and Cowtan, K. (2004) Coot: Model-Building Tools for Molecular Graphics, *Acta Crystallogr. D60*, 2126−2132.
16. Laskowski, R. A., MacArthur, M. W., Moss, D. S., and Thornton, J. M. (1993) PROCHECK: A program to check the stereochemical quality of protein structures, *J. Appl. Crystallogr. 26*, 283−291.
17. Miles, R. W., Tyler, P. C., Furneaux, R. H., Bagdassarian, C. K., and Schramm, V. L. (1998) One-third-the-sites transition-state inhibitors for purine nucleoside phosphorylase, *Biochemistry 37*, 8615−8621.
18. Kim, B. K., Cha, S., and Parks, R. E., Jr. (1968) Purine nucleoside phosphorylase from human erythrocytes. I. Purification and properties, *J. Biol. Chem. 243*, 1763−1770.
19. Gasteiger, E. H. C., Gattiker, A., Duvaud, S., Wilkins, M. R., Appel, R. D., and Bairoch, A. (2005) Protein identification and analysis tools on the ExPASy server, in *The Proteomics Protocols Handbook* (Walker, J. M., Ed.) pp 571−607, Humana Press, Totowa, NJ.
20. Dawson, R. M. C., Elliott, D. C., Elliott, W. H., and Jones, K. M. (1986) *Data for Biochemical Research*, 3rd ed., Clarendon Press, Oxford, U.K.
21. Lim, M.-I., Ren, Y.-Y., Otter, B. A., and Klein, R. S. (1983) Synthesis of "9-deazaguanosine" and other new pyrrolo[3,2-d]-pyrimidine C-nucleosides, *J. Org. Chem. 48*, 780−788.
22. Morrison, J. F., and Walsh, C. T. (1988) The behavior and significance of slow-binding enzyme inhibitors, *Adv. Enzymol. Relat. Areas Mol. Biol. 61*, 201−301.
23. Singh, V., Evans, G. B., Lenz, D. H., Mason, J. M., Clinch, K., Mee, S., Painter, G. F., Tyler, P. C., Furneaux, R. H., Lee, J. E., Howell, P. L., and Schramm, V. L. (2005) Femtomolar transition state analogue inhibitors of 5′-methylthioadenosine/S-adenosylhomocysteine nucleosidase from *Escherichia coli*, *J. Biol. Chem. 280*, 18265−18273.
24. Lewis, B. E., and Schramm, V. L. (2003) Binding equilibrium isotope effects for glucose at the catalytic domain of human brain hexokinase, *J. Am. Chem. Soc. 125*, 4785−4798.
25. Schramm, V. L. (1976) Comparison of initial velocity and binding data for allosteric adenosine monophosphate nucleosidase, *J. Biol. Chem. 251*, 3417−3424.
26. Stoeckler, J. D., Cambor, C., and Parks, R. E., Jr. (1980) Human erythrocytic purine nucleoside phosphorylase: Reaction with sugar-modified nucleoside substrates, *Biochemistry 19*, 102−107.
27. Erion, M. D., Takabayashi, K., Smith, H. B., Kessi, J., Wagner, S., Honger, S., Shames, S. L., and Ealick, S. E. (1997) Purine nucleoside phosphorylase. 1. Structure-function studies, *Biochemistry 36*, 11725−11734.
28. Evans, G. B., Furneaux, R. H., Lewandowicz, A., Schramm, V. L., and Tyler, P. C. (2003) Synthesis of second-generation transition state analogues of human purine nucleoside phosphorylase, *J. Med. Chem. 46*, 5271−5276.
29. Lewandowicz, A., Shi, W., Evans, G. B., Tyler, P. C., Furneaux, R. H., Basso, L. A., Santos, D. S., Almo, S. C., and Schramm, V. L. (2003) Over-the-barrier transition state analogues and crystal structure with *Mycobacterium tuberculosis* purine nucleoside phosphorylase, *Biochemistry 42*, 6057−6066.
30. Canduri, F., dos Santos, D. M., Silva, R. G., Mendes, M. A., Basso, L. A., Palma, M. S., de Azevedo, W. F., and Santos, D. S. (2004) Structures of human purine nucleoside phosphorylase complexed with inosine and ddI, *Biochem. Biophys. Res. Commun. 313*, 907−914.
31. Rossi, C., Picchi, M. P., Tiezzi, E., Corbini, G., and Corti, P. (1990) Conformational and dynamic investigation in solution of inosine and its molecular complex, inosiplex, by proton and carbon NMR spectroscopy, *Magn. Reson. Chem. 28*, 348−354.
32. Davies, D. B., and Rabczenko, A. (1975) Assignment and conformational properties of the exocyclic 5′-hydroxymethyl group of nucleosides by nuclear magnetic resonance spectroscopy, *J. Chem. Soc., Perkin Trans. 2*, 1703−1711.
33. Schweizer, M. P., Banta, E. B., Witkowski, J. T., and Robins, R. K. (1973) Determination of pyrimidine nucleoside syn-anti conformational preference in solution by proton and carbon-13 nuclear magnetic resonance, *J. Am. Chem. Soc. 95*, 3770−3778.
34. Hruska, F. E., Grey, A. A., and Smith, I. C. (1970) A nuclear magnetic resonance study of the molecular conformation of β-pseudouridine in aqueous solution, *J. Am. Chem. Soc. 92*, 4088−4094.

35. Gelbin, A., Schneider, B., Clowney, L., Hsieh, S.-H., Olson, W. K., and Berman, H. M. (1996) Geometric parameters in nucleic acids: Sugar and phosphate constituents, *J. Am. Chem. Soc. 118*, 519−529.
36. Sqaillacote, M., Sheridan, R. S., Chapman, O. L., and Anet, F. A. L. (1975) Spectroscopic detection of the twist-boat conformation of cyclohexane. A direct measurement of the free energy difference between the chair and the twist-boat, *J. Am. Chem. Soc. 97*, 3245−3246.
37. Schramm, V. L. (2005) Enzymatic transition states: Thermodynamics, dynamics and analogue design, *Arch. Biochem. Biophys. 433*, 13−26.
38. Schramm, V. L. (2003) Enzymatic transition state poise and transition state analogues, *Acc. Chem. Res. 36*, 588−596.
39. Lewis, B. E., and Schramm, V. L. (2006) Enzymatic binding isotope effects and the interaction of glucose with hexokinase, in *Isotope Effects in Chemistry and Biology* (Kohen, A., and Limbach, H.-H., Eds.) pp 1019−1053, CRC Press, Boca Raton, FL.
40. Berti, P. J., Blanke, S. R., and Schramm, V. L. (1997) Transition state structure for the hydrolysis of NAD^+ catalyzed by diphtheria toxin. *J. Am. Chem. Soc. 119*, 12079−12088.
41. Scheuring, J., and Schramm, V. L. (1997) Kinetic isotope effect characterization of the transition state for oxidized nicotinamide adenine dinucleotide hydrolysis by pertussis toxin, *Biochemistry 36*, 4526−4534.
42. Parikh, S. L., and Schramm, V. L. (2004) Transition state structure for ADP-ribosylation of eukaryotic elongation factor 2 catalyzed by diphtheria toxin, *Biochemistry 43*, 1204−1212.
43. Schramm, V. L. (1999) Enzymatic transition-state analysis and transition-state analogs, *Methods Enzymol. 308*, 301−355.
44. Kline, P. C., and Schramm, V. L. (1995) Pre-steady-state transition-state analysis of the hydrolytic reaction catalyzed by purine nucleoside phosphorylase, *Biochemistry 34*, 1153−1162.
45. Kline, P. C., and Schramm, V. L. (1993) Purine nucleoside phosphorylase. Catalytic mechanism and transition-state analysis of the arsenolysis reaction, *Biochemistry 32*, 13212−13219.
46. Ruszczycky, M. W., and Anderson, V. E. (2006) Interpretation of V/K isotope effects for enzymatic reactions exhibiting multiple isotopically sensitive steps, *J. Theor. Biol. 243*, 328−342.

BI700147B